Letter

Localization properties in disordered quantum many-body dynamics under continuous measurement

Kazuki Yamamoto [1,2,*] and Ryusuke Hamazaki [3]

[1] *Department of Physics, Tokyo Institute of Technology, Meguro, Tokyo 152-8551, Japan*
[2] *Department of Physics, Kyoto University, Kyoto 606-8502, Japan*
[3] *Nonequilibrium Quantum Statistical Mechanics RIKEN Hakubi Research Team, RIKEN Cluster for Pioneering Research (CPR), RIKEN iTHEMS, Wako, Saitama 351-0198, Japan*

(Received 21 January 2023; revised 24 April 2023; accepted 24 May 2023; published 7 June 2023)

We study the localization properties of continuously monitored dynamics and associated measurement-induced phase transitions in disordered quantum many-body systems on the basis of the quantum trajectory approach. By calculating the fidelity between random quantum trajectories, we demonstrate that the disorder and the measurement can lead to dynamical properties distinct from each other, although both have a power to suppress the entanglement spreading. In particular, in the large-disorder regime with weak measurement, we elucidate that the fidelity exhibits an anomalous power-law decay before saturating to the steady-state value. Furthermore, we propose a general method to access physical quantities for quantum trajectories in continuously monitored dynamics without postselection. It is demonstrated that this scheme drastically reduces the cost of experiments. Our results can be tested in ultracold atoms subject to continuous measurement and open the avenue to study the dynamical properties of localization, which cannot be understood from the stationary properties of the entanglement entropy.

DOI: 10.1103/PhysRevB.107.L220201

Introduction. Localization is an exotic phenomenon where a quantum state fails to spread over the entire Hilbert space. One notable mechanism of localization is the disorder, which prohibits the system from undergoing chaotic dynamics. For example, arbitrary weak disorder in noninteracting one- or two-dimensional systems leads to Anderson localization [1,2], and many-body localization (MBL) transitions occur when the disorder strength exceeds a critical value in interacting systems [3–17]. Recently, MBL has broadened its research arena to open quantum systems [18–25], where it has been demonstrated that unique nonequilibrium phenomena emerge, such as anomalous logarithmic growth of the von Neumann entropy with the scaling collapse normalized by the dissipation rate [18].

Yet another mechanism that has recently attracted great interest is the measurement, which localizes a quantum state in nonunitary quantum circuits [26–52] and continuously monitored systems [53–66]. Remarkably, novel quantum phenomena that have no counterpart in a closed system have been observed: A notable example is the measurement-induced phase transitions (MIPTs) [26–29,67,68], which are typically characterized by phase transitions from a volume law to an area law in the entanglement scaling of the stationary state. Interestingly, a continuously monitored MBL system can be conveyed to the area-law entanglement phase with an infinitesimal measurement strength [69–73]. However, while both the disorder and the measurement localize the wave function and suppress the entanglement spreading, it is still not clear whether they exhibit the same localization properties [74].

In this Letter, we demonstrate that *dynamical* properties of localization induced by the disorder and the measurement are distinct from each other in disordered quantum many-body systems under continuous monitoring. We first elucidate the whole entanglement phase diagram and associated MIPTs with respect to the disorder and the measurement strength. Then, by analyzing the fidelity between random quantum trajectories, we find that two dynamically distinct regimes in the area-law phase appear: The disorder-dominant measurement-induced area-law (DMAL) regime and the measurement-dominant measurement-induced area-law (MMAL) regime (see Fig. 1). We show that the DMAL regime is characterized by an anomalous power-law decay of the fidelity. This distinction is further supported by the long-time dynamics of autocorrelation functions that relax to a disorder-independent value in the MMAL regime, while the DMAL regime exhibits slow dynamics reflecting the initial-state information.

Furthermore, to verify our result in an experimentally accessible way, we propose a general method to obtain physical quantities in the continuously monitored dynamics without postselection. We elucidate that, once jump processes are observed for a single trajectory, we can reproduce the dynamics by repeating the processes of Hamiltonian evolutions and appropriate unitary operations in a closed quantum system. This scheme significantly reduces the experimental cost compared to the postselection of the continuously monitored dynamics.

Measurement-induced phase transitions. We consider disordered interacting hard-core bosons on a one-dimensional

*yamamoto@phys.titech.ac.jp

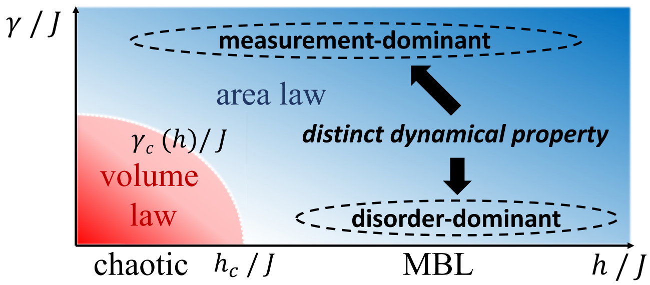

FIG. 1. Entanglement phase diagram with respect to the measurement rate γ/J and the disorder strength h/J in the steady state of the continuously monitored dynamics. Chaotic and MBL phases are separated at the critical disorder strength h_c/J for $\gamma = 0$, and MIPTs at the critical measurement rate $\gamma_c(h)/J$ only occur for $h < h_c$. Though two regimes surrounded by dashed black lines show the area-law entanglement, their dynamical properties of localization are distinct from each other, leading to the MMAL and the DMAL regimes.

lattice subject to open boundary conditions:

$$H = \sum_{j=1}^{L-1} \frac{J}{2}\left(b_{j+1}^{\dagger} b_j + b_{j+1} b_j^{\dagger}\right) + \sum_{j=1}^{L-1} V n_{j+1} n_j + \sum_{j=1}^{L} h_j n_j. \tag{1}$$

Here, b_j ($b_j^{\dagger}$) is the bosonic annihilation (creation) operator satisfying the hard-core constraint $b_j^2 = 0$, $n_j = b_j^{\dagger} b_j$ is the particle number operator, and disorder h_j is randomly chosen from the uniform distribution $h_j \in [-h, h]$. Throughout this Letter, we set $V = J$. Since our aim is to study the measurement-induced trajectory dynamics in open quantum systems, we employ the stochastic Schrödinger equation obeying the marked point process [58,75], which is given in the time interval $[t, t + dt]$ by

$$d|\psi(t)\rangle = \left(-iH_{\text{eff}} + \frac{\gamma}{2} \sum_{j=1}^{L} \langle L_j^{\dagger} L_j \rangle \right) |\psi(t)\rangle dt + \sum_{j=1}^{L} \left(\frac{L_j |\psi(t)\rangle}{\sqrt{\langle L_j^{\dagger} L_j \rangle}} - |\psi(t)\rangle \right) dW_j. \tag{2}$$

Here, $\langle \cdots \rangle$ denotes an expectation value with respect to the quantum state $|\psi(t)\rangle$, and $H_{\text{eff}} = H - \frac{i\gamma}{2} \sum_j L_j^{\dagger} L_j$ is the non-Hermitian Hamiltonian with the jump operator $L_j = n_j$, which describes continuous measurements of the local particle number. We note that a discrete random variable dW_j satisfies $dW_j dW_k = \delta_{jk} dW_j$ and $E[dW_j] = \gamma \langle L_j^{\dagger} L_j \rangle dt$, where $E[\cdot]$ represents an ensemble average over the stochastic process. Importantly, as the total particle number is a conserved quantity, the nonunitary dynamics under H_{eff} is replaced by the unitary evolution under H upon the normalization of the state $|\psi(t)\rangle$ [58]. In the following, we calculate the exact time evolution assuming that the initial state $|\psi_0\rangle$ is prepared in the Néel state $|1010 \cdots\rangle$ at half filling.

Under the quantum trajectory dynamics, the entanglement is built due to the Hamiltonian evolution, while it is erased by the measurement. To obtain entanglement properties and associated MIPTs in the steady state, we start by calculating the von Neumann entropy for a subsystem A, which is defined by

$$S_A = -\text{Tr}_A[\rho_A \ln \rho_A]. \tag{3}$$

Here, $\rho = |\psi\rangle\langle\psi|$ is the density matrix of the system, and the reduced density matrix ρ for a subsystem A is obtained by tracing out over the complement A^c as $\rho_A = \text{Tr}_{A^c} \rho$. Figure 2 shows the half-chain entanglement entropy $\bar{S}_A$ in the steady state with respect to subsystem sizes. Here, $\bar{X} = E_{\text{dis}}[E[X]]$ with E_{dis} denoting the disorder average. We note that the entanglement entropy shows sufficient convergence with respect to time, and all physical quantities in the steady state obtained in this Letter converge with respect to time, trajectory realizations, and disorder realizations with sufficient accuracy. From Figs. 2(a)–2(c), we see that the entanglement exhibits volume-law to area-law MIPTs as the measurement strength is increased in the chaotic phase with weak disorder. On the other hand, in the MBL phase with strong disorder, which is expected to emerge above the critical value $h_c/J \simeq 3.6$ [5,7,76], it has been discussed that any finite measurements force the system to undergo area-law entanglement transitions [69]. We indeed see that the results in Fig. 2(d) show the area-law entanglement scaling qualitatively well. We note that, in Ref. [69], area-law transitions of entanglement entropy were obtained only in the deep MBL phase, which is far above the critical point given by h_c.

To further quantify MIPTs, we calculate the bipartite mutual information I_{AB} between two subregions A and B given by

$$I_{AB} = S_A + S_B - S_{A \cup B}. \tag{4}$$

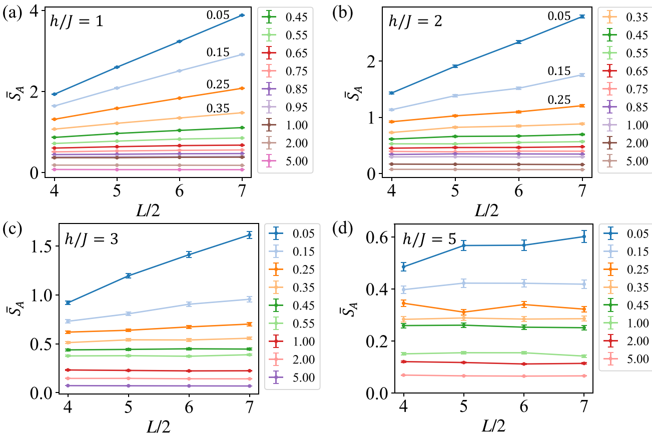

FIG. 2. Half-chain entanglement entropy $\bar{S}_A$ ($A = \{j | 1 \leqslant j \leqslant L/2\}$) in the steady state with respect to $L/2$ for (a) $h/J = 1$, (b) $h/J = 2$, (c) $h/J = 3$, and (d) $h/J = 5$. The legend shows γ/J. The entanglement exhibits MIPTs for $h < h_c$, while it immediately undergoes area-law transitions for $h > h_c$. Steady state is reached at $\gamma t = 1000$ in (a)–(c), and $\gamma t = 2000$ in (d) with the average over 300×100 realizations. Hereafter, we use the notation "$n \times m$ realizations" to represent that m-trajectory samplings are performed for each n-disorder sampling.

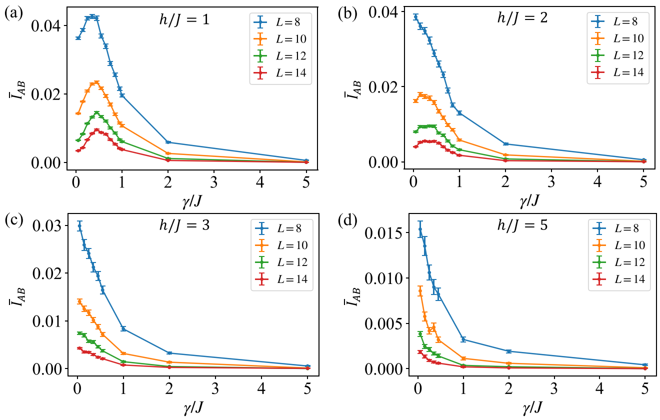

FIG. 3. Mutual information $\bar{I}_{AB}$ ($A = \{1\}$, $B = \{L/2 + 1\}$) with respect to γ/J in the steady state for (a) $h/J = 1$, (b) $h/J = 2$, (c) $h/J = 3$, and (d) $h/J = 5$. Critical points of MIPTs are evaluated from the peak of $\bar{I}_{AB}$. Steady state is reached at $\gamma t = 1000$ in (a)–(c), and $\gamma t = 2000$ in (d) with the average over 300×100 realizations.

Previous studies have found that the mutual information (4) exhibits a peak at the critical point of MIPTs with respect to the measurement rate [29]. Figure 3 shows the mutual information in the steady state. We note that the choice of the distance between A and B does not affect the qualitative argument if they are located at a distance of the order of L; here, we take $A = \{1\}$ and $B = \{L/2 + 1\}$. As clearly seen from Figs. 3(a)–3(d), the peak of $\bar{I}_{AB}$ gradually shifts towards lower γ/J as the disorder strength h/J is increased, and in the MBL phase, the critical value of MIPTs $\gamma_c(h)/J$ becomes zero irrespective of the disorder strength. From these results, we have elucidated the phase diagram shown in Fig. 1 (see Supplemental Material [77] for the quantitative diagram). We note that previous works on MIPTs in MBL systems have not obtained the entire phase diagram in Fig. 1 [69–73].

Dynamical properties of localization. Although the stationary state displays the area-law entanglement in the greater part of the phase diagram, it is not clear whether the regime near the unitary MBL phase (DMAL regime) and the one far from the unitary phase (MMAL regime) dynamically show the same property (see Fig. 1). In order to clarify this problem, we analyze the fidelity that describes the overlap between independent random quantum trajectories $|\psi(t)\rangle$ and $|\psi'(t)\rangle$ for each disorder given by

$$F(t) = |\langle\psi(t)|\psi'(t)\rangle|, \tag{5}$$

and study its average over disorder and trajectories [78]. We note that, as the (normalized) states $|\psi(t)\rangle$ and $|\psi'(t)\rangle$ in Eq. (5) are prepared for the same disorder distribution, the fidelity stays at $F(t) = 1$ for $\gamma = 0$ if the dynamics starts from an identical initial state. Remarkably, we find that the fidelity in the DMAL regime $\bar{F}_{\rm MBL}(t)$ reveals an anomalous power-law behavior for times $\gamma t \gg 1$ before saturating to the steady-state value as

$$\bar{F}_{\rm MBL}(t) \propto \left(\frac{1}{\gamma t}\right)^{\alpha}. \tag{6}$$

In Fig. 4, we have calculated the dynamics of the fidelity in the DMAL regime, where we have set $h/J = 10$ and $\gamma/J = 0.05$.

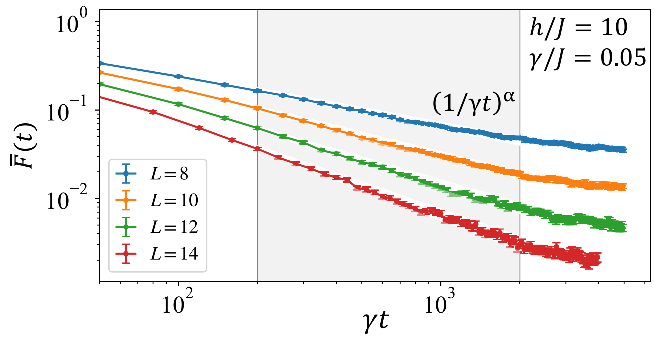

FIG. 4. Log-log plot of the dynamics of the fidelity $\bar{F}(t)$ with respect to γt in the DMAL regime. The shaded region, which is a guide to the eye, shows the power-law behavior of the fidelity. The parameters are set to $h/J = 10$ and $\gamma/J = 0.05$, and the disorder average is taken over 300 realizations. For each fixed disorder, we take 50 pairs of trajectories with respect to $|\psi(t)\rangle$ and $|\psi'(t)\rangle$.

We have obtained the exponent α from the power-law fitting of the data (taken in the time interval $200 \leqslant \gamma t \leqslant 2000$) as $\alpha = 0.55, 0.74, 0.93, 1.07$ (± 0.01) for $L = 8, 10, 12, 14$, respectively. As shown in Fig. S5 in the Supplemental Material, the exponent α seems to be proportional to L for small system sizes. On the other hand, as we depart from the DMAL regime, the numerical results demonstrate that this power-law dependence of the fidelity is smeared and finally vanishes in the MMAL regime [77]. This is because the time that the power-law decay should end becomes shorter than the typical timescale of the system such as $1/J$.

Thus, we demonstrate that, though both the disorder and the measurement localize the wave function in the steady state, the speed of relaxation dynamics in the DMAL regime is slow enough to exhibit the power-law behavior of the fidelity. We also find that the overlap between random quantum trajectories in the steady state is suppressed by the disorder and the measurement, while the fidelity is made to be zero in the limit $L \to \infty$ in the entire phase diagram [77]. These results conclude that the dynamical property in the DMAL regime is distinct from that in the MMAL regime.

We note that Eq. (6) is reminiscent of the logarithmic growth of the von Neumann entropy in the MBL system following the Lindblad master equation [18]. In Ref. [18], it is pointed out that the von Neumann entropy of the whole system $S_{\rm MBL}^{\rm Lind}(t)$ exhibits the logarithmic growth for times $\gamma t \gg 1$ before saturation as $E_{\rm dis}[S_{\rm MBL}^{\rm Lind}(t)] \propto \beta \log(\gamma t)$. As the density matrix in the Lindblad equation $\rho_{\rm Lind}(t)$ is related to that in the trajectory dynamics $\rho(t)$ as $\rho_{\rm Lind}(t) = E[\rho(t)]$, we find that the trajectory average of the squared fidelity in Eq. (5) is given by $E[F(t)^2] = {\rm Tr}[\rho_{\rm Lind}(t)^2]$. Assuming that the second Rényi entropy $S_2(t) = -\log {\rm Tr}[\rho(t)^2]$ behaves similarly as the von Neumann entropy, we obtain $E_{\rm dis}[\log E[F_{\rm MBL}(t)^2]] = -E_{\rm dis}[S_{2\,\rm MBL}^{\rm Lind}(t)] \propto \log(1/\gamma t)^{\beta}$. If $E_{\rm dis}$ commutes with log and the squared fidelity displays similar behavior as the fidelity, we arrive at Eq. (6). We note that $\beta \propto L\sqrt{J/h}$ is reported in Ref. [18], and this value is consistent with the fitting data of the exponent α in Eq. (6), which seems to increase as we increase the system size L. However, we stress that $E[F_{\rm MBL}(t)]$ cannot exactly reduce to the quantity calculated from the averaged dynamics of $\rho_{\rm Lind}(t)$.

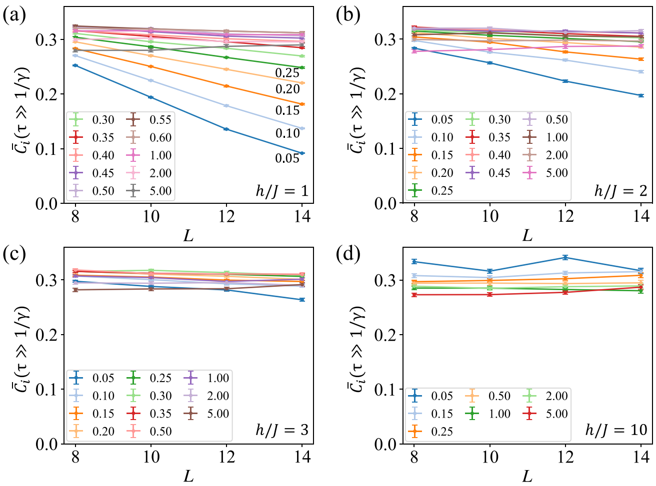

FIG. 5. System-size dependence of the autocorrelation function $\bar{C}_i(\tau)$ $(i = L/2 + 1)$ in the long-time regime $\tau \gg 1/\gamma$, which takes a disorder-independent value in the MMAL regime and shows slow relaxation reflecting the initial-state information in the DMAL regime. The legend shows γ/J. The starting point of the autocorrelation is taken at $\gamma t = 667$ in (a)–(c), and $\gamma t = 2000$ in (d). We set $\gamma\tau = 333$ in (a)–(c), and $\gamma\tau = 1000$ in (d), and take an average over 300×100 realizations for (a) $h/J = 1$, (b) $h/J = 2$, and (c) $h/J = 3$, and 300×50 realizations for (d) $h/J = 10$.

Furthermore, we study the dynamics of the following autocorrelation function,

$$C_i(\tau) = |\lim_{t\to\infty} \langle\psi(t+\tau)|n_i|\psi^{n_i}(t+\tau)\rangle|, \tag{7}$$

where $|\psi^{n_i}(t+\tau)\rangle$ stands for a quantum state that gives the same realization of quantum jump processes as $|\psi(t+\tau)\rangle$, while the particle number operator n_i is inserted into the dynamics at some time t [77]. Here, we note that the normalization condition of $|\psi^{n_i}(t+\tau)\rangle$ is given by $||\,|\psi^{n_i}(t+\tau)\rangle\,|| = ||n_i|\psi(t)\rangle||$. The autocorrelation function (7) describes how the particle number operator overlaps with itself under the dynamics from the steady state. Figure 5 shows the autocorrelation function in the long-time regime for the weak disorder case [Figs. 5(a)–5(c)] and the strong disorder case [Fig. 5(d)]. Importantly, we find a characteristic phenomenon that the long-time autocorrelation takes the disorder-independent value around $\bar{C}_i(\tau \gg 1/\gamma) \simeq 0.3$ in the MMAL regime for the large measurement rate γ/J. On the other hand, as shown in Fig. 5(d), we see that the autocorrelation function in the DMAL regime with weak measurement shows a slow relaxation reflecting the information about the initial Néel state (see the plot for $\gamma/J = 0.05$). Here, we note that, as we take the site i in $C_i(\tau)$ to be $i = L/2 + 1$, the dynamics from $t = 0$ starts from an up spin for $L = 8$, 12, and from a down spin for $L = 10$, 14. The difference between the relaxation dynamics means that the initial-state information in the dynamical overlap of the particle number operator is smeared faster in the MMAL regime, where the localization effect caused by the measurement exceeds the one caused by the disorder. Since the dynamics in the DMAL regime is slow enough as shown in the power-law decay of the fidelity in Eq. (6), the slow relaxation of the autocorrelation function agrees with it. In addition, in the volume-law phase [see Figs. 5(a)–5(c)], we find that $\bar{C}_i(\tau \gg 1/\gamma)$ seems to become zero in the limit $L \to \infty$. Since the eigenstate thermalization hypothesis [79] guarantees $E_{\mathrm{dis}}[C_i(\tau\to\infty)] \to 0.25$ under the unitary dynamics with $\gamma = 0$ in the chaotic phase, it is surprising that any finite measurement immediately changes the value of $\bar{C}_i(\tau \gg 1/\gamma)$ to zero. To analyze the phenomena in detail, we have further calculated $C'_i(\tau) = |\lim_{t\to\infty}\langle\psi(t+\tau)|\psi^{n_i}(t+\tau)\rangle|$ and found that the behavior of $\bar{C}'_i(\tau \gg 1/\gamma)$ is qualitatively similar to that of $\bar{C}_i(\tau \gg 1/\gamma)$ (see Supplemental Material [77] for detailed results). Thus, we conclude that the behavior shown in Fig. 5 stems from that of the overlap between the trajectories $|\psi^{n_i}(t+\tau)\rangle$ and $|\psi(t+\tau)\rangle$, though the detailed analysis is left for future work.

Accessing physical quantities without postselection. Generally, to experimentally realize the trajectory dynamics, we need to postselect special measurement outcomes so as to collect the trajectories that reproduce the same jump processes (see below). However, under continuously monitored dynamics, such experiments require an extremely large number of trials including the factor $[1/(\gamma L\Delta t)]^N \times L^N$ for a single quantum trajectory, where $\gamma L\Delta t =: \epsilon \ll 1$ represents the accuracy of reproducing the same jump timing and N is the number of quantum jumps. To eliminate this factor, we focus on the fact that $\sum_i L_i^\dagger L_i = \sum_i n_i$ is a conserved quantity under the measurement $L_i = n_i$ and propose a general way to realize the trajectory dynamics without postselection [67,80–86] (see Supplemental Material [77] for details).

The stochastic dynamics (2) is constructed from the unitary time evolution described by the Hermitian Hamiltonian (1) and the measurement process given by the particle number operator $L_i = n_i$. Then, the evolved state for a single quantum trajectory is written as $|\psi(t)\rangle \propto e^{-iH(t-t_N)} n_{i_N} e^{-iH(t_N-t_{N-1})} n_{i_{N-1}} \cdots e^{-iHt_1}|\psi_0\rangle$, where $\{t_j, i_j\}$ $(j = 1, \ldots, N)$ is a set of the time and the site of quantum jump processes. Importantly, by using this fact and that the particle number operator is given by $n_i = \sigma_i^z/2 + 1/2$, where σ_i^z is the Pauli matrix, we can decompose the physical quantities into a set of terms including a finite number of σ_i^z operators as follows. For example, the fidelity (5) is constructed from terms such as

$$\langle\psi_0|e^{iHt_1}\sigma_{i_1}^z e^{iH(t_2-t_1)}\cdots e^{-iH(t'_2-t'_1)}\sigma_{i'_1}^z e^{-iHt'_1}|\psi_0\rangle, \tag{8}$$

where $\{t'_j, i'_j\}$ $(j = 1, \ldots, N')$ is a set of jump processes corresponding to $|\psi'(t)\rangle$ and at most $N + N'$ number of σ_i^z operators appear. Then, once the jump processes $\{t_j, i_j\}$ and $\{t'_j, i'_j\}$ are obtained, we can reproduce the expectation value (8) by evolving the state under the Hermitian Hamiltonian H and applying a σ^z unitary operation in a closed system. We note that, as the Rényi entropy has been experimentally observed by using the SWAP operation [87–90], the above method is readily applicable to obtain the entanglement entropy that determines MIPTs. Thus, we can obtain the physical quantities discussed in this Letter without postselection [67,80–86] and can significantly reduce the cost stemming from the factor $(1/\epsilon)^N \times L^N$.

Conclusion. We have elucidated that dynamical properties of localization induced by the measurement and the disorder are distinct from each other. In particular, in the large-disorder regime with weak measurement, the dynamics of the fidelity is highlighted by the anomalous power-law decay. Our results are readily observed in ultracold atoms, by first combining the off-resonant probe light and the quantum-gas microscopy to realize the continuously monitored dynamics [91], and then applying our postselection-free probe method without dissipation. It should be noted that there has been a heuristic argument regarding the existence of the MBL phase in the thermodynamic limit [76]. However, we emphasize that mesoscopic systems such as ultracold atoms in an optical lattice have experimentally demonstrated the existence of chaotic-MBL transitions [17]. Thus, our results are still relevant to experiments regardless of the existence of the MBL phase in the thermodynamic limit. Regarding the finite-size effect, although our calculation is restricted to small system sizes due to numerical limitation, it is important to study the precise system-size dependence of the power-law exponent of the fidelity. Though it is numerically difficult to find critical points in the dynamics of autocorrelation functions, it deserves to study how MIPTs of entanglement are related to them. Moreover, as a similar phase diagram has been obtained in MBL of Liouvillian eigenstates [23], it is of interest to investigate its relation to MIPTs. Last but not least, since localization properties of monitored free fermions that exhibit Anderson localization have been recently studied [74,92,93], it is also interesting how dynamical properties in monitored MBL systems are related to those in monitored Anderson localized systems.

Acknowledgments. We are grateful to Norio Kawakami for encouraging our research. K.Y. also thanks Masaya Nakagawa for fruitful discussions. The numerical calculations were partly carried out with the help of QuSpin [94]. We also thank MACS program in Kyoto University for stimulating our collaborations. K.Y. was supported by WISE Program, MEXT and JSPS KAKENHI Grant-in-Aid for JSPS fellows Grant No. JP20J21318.

[1] P. W. Anderson, Absence of diffusion in certain random lattices, Phys. Rev. **109**, 1492 (1958).

[2] E. Abrahams, P. W. Anderson, D. C. Licciardello, and T. V. Ramakrishnan, Scaling Theory of Localization: Absence of Quantum Diffusion in Two Dimensions, Phys. Rev. Lett. **42**, 673 (1979).

[3] D. M. Basko, I. L. Aleiner, and B. L. Altshuler, Metal–insulator transition in a weakly interacting many-electron system with localized single-particle states, Ann. Phys. **321**, 1126 (2006).

[4] M. Žnidarič, T. Prosen, and P. Prelovšek, Many-body localization in the Heisenberg XXZ magnet in a random field, Phys. Rev. B **77**, 064426 (2008).

[5] A. Pal and D. A. Huse, Many-body localization phase transition, Phys. Rev. B **82**, 174411 (2010).

[6] J. H. Bardarson, F. Pollmann, and J. E. Moore, Unbounded Growth of Entanglement in Models of Many-Body Localization, Phys. Rev. Lett. **109**, 017202 (2012).

[7] D. J. Luitz, N. Laflorencie, and F. Alet, Many-body localization edge in the random-field Heisenberg chain, Phys. Rev. B **91**, 081103(R) (2015).

[8] M. Serbyn, Z. Papić, and D. A. Abanin, Criterion for Many-Body Localization-Delocalization Phase Transition, Phys. Rev. X **5**, 041047 (2015).

[9] J. Z. Imbrie, Diagonalization and Many-Body Localization for a Disordered Quantum Spin Chain, Phys. Rev. Lett. **117**, 027201 (2016).

[10] J. Z. Imbrie, On many-body localization for quantum spin chains, J. Stat. Phys. **163**, 998 (2016).

[11] S. D. Geraedts, R. Nandkishore, and N. Regnault, Many-body localization and thermalization: Insights from the entanglement spectrum, Phys. Rev. B **93**, 174202 (2016).

[12] D. J. Luitz and Y. B. Lev, The ergodic side of the many-body localization transition, Ann. Phys. **529**, 1600350 (2017).

[13] R. Nandkishore and D. A. Huse, Many-body localization and thermalization in quantum statistical mechanics, Annu. Rev. Condens. Matter Phys. **6**, 15 (2015).

[14] E. Altman and R. Vosk, Universal dynamics and renormalization in many-body-localized systems, Annu. Rev. Condens. Matter Phys. **6**, 383 (2015).

[15] D. A. Abanin, E. Altman, I. Bloch, and M. Serbyn, Colloquium: Many-body localization, thermalization, and entanglement, Rev. Mod. Phys. **91**, 021001 (2019).

[16] J. Smith, A. Lee, P. Richerme, B. Neyenhuis, P. W. Hess, P. Hauke, M. Heyl, D. A. Huse, and C. Monroe, Many-body localization in a quantum simulator with programmable random disorder, Nat. Phys. **12**, 907 (2016).

[17] J.-y. Choi, S. Hild, J. Zeiher, P. Schauß, A. Rubio-Abadal, T. Yefsah, V. Khemani, D. A. Huse, I. Bloch, and C. Gross, Exploring the many-body localization transition in two dimensions, Science **352**, 1547 (2016).

[18] E. Levi, M. Heyl, I. Lesanovsky, and J. P. Garrahan, Robustness of Many-Body Localization in the Presence of Dissipation, Phys. Rev. Lett. **116**, 237203 (2016).

[19] M. H. Fischer, M. Maksymenko, and E. Altman, Dynamics of a Many-Body-Localized System Coupled to a Bath, Phys. Rev. Lett. **116**, 160401 (2016).

[20] M. V. Medvedyeva, T. Prosen, and M. Žnidarič, Influence of dephasing on many-body localization, Phys. Rev. B **93**, 094205 (2016).

[21] H. P. Lüschen, P. Bordia, S. S. Hodgman, M. Schreiber, S. Sarkar, A. J. Daley, M. H. Fischer, E. Altman, I. Bloch, and U. Schneider, Signatures of Many-Body Localization in a Controlled Open Quantum System, Phys. Rev. X **7**, 011034 (2017).

[22] R. Hamazaki, K. Kawabata, and M. Ueda, Non-Hermitian Many-Body Localization, Phys. Rev. Lett. **123**, 090603 (2019).

[23] R. Hamazaki, M. Nakagawa, T. Haga, and M. Ueda, Lindbladian many-body localization, arXiv:2206.02984.

[24] E. P. van Nieuwenburg, J. Y. Malo, A. J. Daley, and M. H. Fischer, Dynamics of many-body localization in the presence of particle loss, Quantum Sci. Technol. **3**, 01LT02 (2018).

[25] J. Ren, Q. Li, W. Li, Z. Cai, and X. Wang, Noise-Driven Universal Dynamics towards an Infinite Temperature State, Phys. Rev. Lett. **124**, 130602 (2020).

[26] Y. Li, X. Chen, and M. P. A. Fisher, Quantum Zeno effect and the many-body entanglement transition, Phys. Rev. B **98**, 205136 (2018).

[27] A. Chan, R. M. Nandkishore, M. Pretko, and G. Smith, Unitary-projective entanglement dynamics, Phys. Rev. B **99**, 224307 (2019).

[28] B. Skinner, J. Ruhman, and A. Nahum, Measurement-Induced Phase Transitions in the Dynamics of Entanglement, Phys. Rev. X **9**, 031009 (2019).

[29] Y. Li, X. Chen, and M. P. A. Fisher, Measurement-driven entanglement transition in hybrid quantum circuits, Phys. Rev. B **100**, 134306 (2019).

[30] C.-M. Jian, Y.-Z. You, R. Vasseur, and A. W. W. Ludwig, Measurement-induced criticality in random quantum circuits, Phys. Rev. B **101**, 104302 (2020).

[31] M. P. Fisher, V. Khemani, A. Nahum, and S. Vijay, Random quantum circuits, Annu. Rev. Condens. Matter Phys. **14**, 335 (2023).

[32] Q. Tang and W. Zhu, Measurement-induced phase transition: A case study in the nonintegrable model by density-matrix renormalization group calculations, Phys. Rev. Res. **2**, 013022 (2020).

[33] S. Choi, Y. Bao, X.-L. Qi, and E. Altman, Quantum Error Correction in Scrambling Dynamics and Measurement-Induced Phase Transition, Phys. Rev. Lett. **125**, 030505 (2020).

[34] Y. Bao, S. Choi, and E. Altman, Theory of the phase transition in random unitary circuits with measurements, Phys. Rev. B **101**, 104301 (2020).

[35] M. J. Gullans and D. A. Huse, Dynamical Purification Phase Transition Induced by Quantum Measurements, Phys. Rev. X **10**, 041020 (2020).

[36] M. J. Gullans and D. A. Huse, Scalable Probes of Measurement-Induced Criticality, Phys. Rev. Lett. **125**, 070606 (2020).

[37] S. Vijay, Measurement-driven phase transition within a volume-law entangled phase, arXiv:2005.03052.

[38] M. Szyniszewski, A. Romito, and H. Schomerus, Entanglement transition from variable-strength weak measurements, Phys. Rev. B **100**, 064204 (2019).

[39] X. Turkeshi, R. Fazio, and M. Dalmonte, Measurement-induced criticality in $(2+1)$-dimensional hybrid quantum circuits, Phys. Rev. B **102**, 014315 (2020).

[40] A. Zabalo, M. J. Gullans, J. H. Wilson, S. Gopalakrishnan, D. A. Huse, and J. H. Pixley, Critical properties of the measurement-induced transition in random quantum circuits, Phys. Rev. B **101**, 060301(R) (2020).

[41] R. Fan, S. Vijay, A. Vishwanath, and Y.-Z. You, Self-organized error correction in random unitary circuits with measurement, Phys. Rev. B **103**, 174309 (2021).

[42] Y. Li, X. Chen, A. W. W. Ludwig, and M. P. A. Fisher, Conformal invariance and quantum nonlocality in critical hybrid circuits, Phys. Rev. B **104**, 104305 (2021).

[43] O. Lunt, M. Szyniszewski, and A. Pal, Measurement-induced criticality and entanglement clusters: A study of one-dimensional and two-dimensional Clifford circuits, Phys. Rev. B **104**, 155111 (2021).

[44] S. Sang and T. H. Hsieh, Measurement-protected quantum phases, Phys. Rev. Res. **3**, 023200 (2021).

[45] M. Block, Y. Bao, S. Choi, E. Altman, and N. Y. Yao, Measurement-Induced Transition in Long-Range Interacting Quantum Circuits, Phys. Rev. Lett. **128**, 010604 (2022).

[46] J. Côté and S. Kourtis, Entanglement Phase Transition with Spin Glass Criticality, Phys. Rev. Lett. **128**, 240601 (2022).

[47] P. Sierant and X. Turkeshi, Universal Behavior beyond Multifractality of Wave Functions at Measurement-Induced Phase Transitions, Phys. Rev. Lett. **128**, 130605 (2022).

[48] A. Zabalo, M. J. Gullans, J. H. Wilson, R. Vasseur, A. W. W. Ludwig, S. Gopalakrishnan, D. A. Huse, and J. H. Pixley, Operator Scaling Dimensions and Multifractality at Measurement-Induced Transitions, Phys. Rev. Lett. **128**, 050602 (2022).

[49] H. Oshima and Y. Fuji, Charge fluctuation and charge-resolved entanglement in a monitored quantum circuit with $U(1)$ symmetry, Phys. Rev. B **107**, 014308 (2023).

[50] S. Wu and Z. Cai, Feedback-induced interactive dynamics: Unitary but dissipative evolution, arXiv:2211.09291.

[51] Z. Weinstein, S. P. Kelly, J. Marino, and E. Altman, Scrambling transition in a radiative random unitary circuit, arXiv:2210.14242.

[52] S. P. Kelly, U. Poschinger, F. Schmidt-Kaler, M. Fisher, and J. Marino, Coherence requirements for quantum communication from hybrid circuit dynamics, arXiv:2210.11547.

[53] X. Cao, A. Tilloy, and A. De Luca, Entanglement in a fermion chain under continuous monitoring, SciPost Phys. **7**, 024 (2019).

[54] O. Alberton, M. Buchhold, and S. Diehl, Entanglement Transition in a Monitored Free-Fermion Chain: From Extended Criticality to Area Law, Phys. Rev. Lett. **126**, 170602 (2021).

[55] X. Turkeshi, A. Biella, R. Fazio, M. Dalmonte, and M. Schiró, Measurement-induced entanglement transitions in the quantum Ising chain: From infinite to zero clicks, Phys. Rev. B **103**, 224210 (2021).

[56] X. Turkeshi, M. Dalmonte, R. Fazio, and M. Schirò, Entanglement transitions from stochastic resetting of non-Hermitian quasiparticles, Phys. Rev. B **105**, L241114 (2022).

[57] G. Piccitto, A. Russomanno, and D. Rossini, Entanglement transitions in the quantum Ising chain: A comparison between different unravelings of the same Lindbladian, Phys. Rev. B **105**, 064305 (2022).

[58] Y. Fuji and Y. Ashida, Measurement-induced quantum criticality under continuous monitoring, Phys. Rev. B **102**, 054302 (2020).

[59] S. Goto and I. Danshita, Measurement-induced transitions of the entanglement scaling law in ultracold gases with controllable dissipation, Phys. Rev. A **102**, 033316 (2020).

[60] M. Szyniszewski, A. Romito, and H. Schomerus, Universality of Entanglement Transitions from Stroboscopic to Continuous Measurements, Phys. Rev. Lett. **125**, 210602 (2020).

[61] S.-K. Jian, C. Liu, X. Chen, B. Swingle, and P. Zhang, Measurement-Induced Phase Transition in the Monitored Sachdev-Ye-Kitaev Model, Phys. Rev. Lett. **127**, 140601 (2021).

[62] M. Van Regemortel, Z.-P. Cian, A. Seif, H. Dehghani, and M. Hafezi, Entanglement Entropy Scaling Transition under Competing Monitoring Protocols, Phys. Rev. Lett. **126**, 123604 (2021).

[63] E. V. H. Doggen, Y. Gefen, I. V. Gornyi, A. D. Mirlin, and D. G. Polyakov, Generalized quantum measurements with matrix product states: Entanglement phase transition and clusterization, Phys. Rev. Res. **4**, 023146 (2022).

[64] T. Minato, K. Sugimoto, T. Kuwahara, and K. Saito, Fate of Measurement-Induced Phase Transition in Long-Range Interactions, Phys. Rev. Lett. **128**, 010603 (2022).

[65] T. Müller, S. Diehl, and M. Buchhold, Measurement-Induced Dark State Phase Transitions in Long-Ranged Fermion Systems, Phys. Rev. Lett. **128**, 010605 (2022).
[66] M. Buchhold, Y. Minoguchi, A. Altland, and S. Diehl, Effective Theory for the Measurement-Induced Phase Transition of Dirac Fermions, Phys. Rev. X **11**, 041004 (2021).
[67] C. Noel, P. Niroula, D. Ahu, A. Risinger, L. Egan, D. Biswas, M. Cetina, A. V. Gorshkov, M. Gullans, D. A. Huse, and C. Monroe, Measurement-induced quantum phases realized in a trapped-ion quantum computer, Nat. Phys. **18**, 760 (2022).
[68] J. M. Koh, S.-N. Sun, M. Motta, and A. J. Minnich, Experimental realization of a measurement-induced entanglement phase transition on a superconducting quantum processor, arXiv:2203.04338.
[69] O. Lunt and A. Pal, Measurement-induced entanglement transitions in many-body localized systems, Phys. Rev. Res. **2**, 043072 (2020).
[70] M. Ippoliti, M. J. Gullans, S. Gopalakrishnan, D. A. Huse, and V. Khemani, Entanglement Phase Transitions in Measurement-Only Dynamics, Phys. Rev. X **11**, 011030 (2021).
[71] T. Boorman, M. Szyniszewski, H. Schomerus, and A. Romito, Diagnostics of entanglement dynamics in noisy and disordered spin chains via the measurement-induced steady-state entanglement transition, Phys. Rev. B **105**, 144202 (2022).
[72] T.-C. Lu and T. Grover, Spacetime duality between localization transitions and measurement-induced transitions, PRX Quantum **2**, 040319 (2021).
[73] A. Zabalo, J. H. Wilson, M. J. Gullans, R. Vasseur, S. Gopalakrishnan, D. A. Huse, and J. Pixley, Infinite-randomness criticality in monitored quantum dynamics with static disorder, arXiv:2205.14002.
[74] M. Szyniszewski, O. Lunt, and A. Pal, Disordered monitored free fermions, arXiv:2211.02534.
[75] A. J. Daley, Quantum trajectories and open many-body quantum systems, Adv. Phys. **63**, 77 (2014).
[76] There has been an argument regarding the critical point of MBL transitions. For example, in Refs. [95,96], a possibility of a shift of the transition point to a much larger value than the one found in numerics is pointed out on the basis of the analysis of the avalanche instability [97].
[77] See Supplemental Material at http://link.aps.org/supplemental/10.1103/PhysRevB.107.L220201 for the numerical algorithm for the marked point process, the steady-state properties in the MBL phase, the phase diagram for $L = 14$, the dynamics and the stationary value of the fidelity in the whole phase diagram, further explanations and results on the autocorrelation function, and estimation of the cost of postselection under continuous measurement.
[78] K. Życzkowski and H.-J. Sommers, Average fidelity between random quantum states, Phys. Rev. A **71**, 032313 (2005).
[79] M. Rigol, V. Dunjko, and M. Olshanii, Thermalization and its mechanism for generic isolated quantum systems, Nature (London) **452**, 854 (2008).
[80] M. Ippoliti and V. Khemani, Postselection-Free Entanglement Dynamics via Spacetime Duality, Phys. Rev. Lett. **126**, 060501 (2021).
[81] M. Ippoliti, T. Rakovszky, and V. Khemani, Fractal, Logarithmic, and Volume-Law Entangled Nonthermal Steady States via Spacetime Duality, Phys. Rev. X **12**, 011045 (2022).
[82] Y. Li, Y. Zou, P. Glorioso, E. Altman, and M. Fisher, Cross entropy benchmark for measurement-induced phase transitions, Phys. Rev. Lett. **130**, 220404 (2023).
[83] X. Feng, B. Skinner, and A. Nahum, Measurement-induced phase transitions on dynamical quantum trees, arXiv:2210.07264.
[84] H. Dehghani, A. Lavasani, M. Hafezi, and M. J. Gullans, Neural-network decoders for measurement induced phase transitions, arXiv:2204.10904.
[85] S. J. Garratt, Z. Weinstein, and E. Altman, Measurements conspire nonlocally to restructure critical quantum states, arXiv:2207.09476.
[86] M. Buchhold, T. Mueller, and S. Diehl, Revealing measurement-induced phase transitions by pre-selection, arXiv:2208.10506.
[87] M. B. Hastings, I. González, A. B. Kallin, and R. G. Melko, Measuring Renyi Entanglement Entropy in Quantum Monte Carlo Simulations, Phys. Rev. Lett. **104**, 157201 (2010).
[88] D. A. Abanin and E. Demler, Measuring Entanglement Entropy of a Generic Many-Body System with a Quantum Switch, Phys. Rev. Lett. **109**, 020504 (2012).
[89] A. J. Daley, H. Pichler, J. Schachenmayer, and P. Zoller, Measuring Entanglement Growth in Quench Dynamics of Bosons in an Optical Lattice, Phys. Rev. Lett. **109**, 020505 (2012).
[90] R. Islam, R. Ma, P. M. Preiss, M. Eric Tai, A. Lukin, M. Rispoli, and M. Greiner, Measuring entanglement entropy in a quantum many-body system, Nature (London) **528**, 77 (2015).
[91] Y. Ashida, S. Furukawa, and M. Ueda, Quantum critical behavior influenced by measurement backaction in ultracold gases, Phys. Rev. A **94**, 053615 (2016).
[92] P. Pöpperl, I. V. Gornyi, and Y. Gefen, Measurements on an Anderson chain, Phys. Rev. B **107**, 174203 (2023).
[93] In Ref. [74], difference of localization properties between Anderson localized unitary phase and the measurement-induced area-law regime at weak measurement strength has been studied.
[94] P. Weinberg and M. Bukov, QuSpin: A Python package for dynamics and exact diagonalisation of quantum many body systems part I: Spin chains, SciPost Phys. **2**, 003 (2017).
[95] A. Morningstar, L. Colmenarez, V. Khemani, D. J. Luitz, and D. A. Huse, Avalanches and many-body resonances in many-body localized systems, Phys. Rev. B **105**, 174205 (2022).
[96] D. Sels, Bath-induced delocalization in interacting disordered spin chains, Phys. Rev. B **106**, L020202 (2022).
[97] W. De Roeck and F. Huveneers, Stability and instability towards delocalization in many-body localization systems, Phys. Rev. B **95**, 155129 (2017).